NANO LETTERS

2006
Vol. 6, No. 3
361−364

Nanolithography Using High Transmission Nanoscale Bowtie Apertures

Liang Wang, Sreemanth M. Uppuluri, Eric X. Jin, and Xianfan Xu*

School of Mechanical Engineering, Purdue University, West Lafayette, Indiana 47907

Received December 1, 2005; Revised Manuscript Received January 11, 2006

ABSTRACT

We demonstrate that bowtie apertures can be used for contact lithography to achieve nanometer scale resolution. The bowtie apertures with a 30 nm gap size are fabricated in aluminum thin films coated on quartz substrates. Lithography results show that holes of sub-50-nm dimensions can be produced in photoresist by illuminating the apertures with a 355 nm laser beam polarized in the direction across the gap. Experimental results show enhanced transmission and light concentration of bowtie apertures compared to square and rectangular apertures of the same opening area. Finite different time domain simulations are used to explain the experimental results.

Nanolithography is a key technique for nanoscale pattern definition. As alternatives to electron beam lithography, a number of low-cost lithography methods including evanescent near-field photolithography,[1,2] nanoimprint lithography,[3] scanning probe lithography,[4] and surface plasmon assisted nanolithography[5−7] have been explored. Utilizing the confined evanescent optical field, near-field photolithography extends the capability of traditional photolithography beyond the diffraction limit. However, near-field nanolithography using a nanometer-scale circular- or square-shaped aperture as the mask suffers from extremely low light transmission[8] and poor contrast due to the wavelength cutoff effect. Deep or EUV light sources of shorter wavelengths might be used to extend the methodology of the traditional optical lithography, but the cost and complexity of the optical system will increase dramatically. Recently, numerical[9,10] and experimental[11,12] studies showed that extraordinary optical transmission and nanoscale spatial resolution could be achieved with the use of C- and H-shaped ridge apertures benefiting from the waveguide propagation mode confined in the gap between the ridges.

This work focuses on a particular type of ridge aperture, the bowtie aperture. Numerical studies on bowtie apertures[13,14] have shown their great potential in concentrating light to a superconfined spot with intense local field. A bowtie aperture is the counterpart of a bowtie antenna as shown in Figure 1. Both of these consist of two arms and a small gap formed by two sharp tips pointing toward each other. The bowtie antenna was first proposed in the microwave regime as an efficient near-field probe,[15] and recently realized in nanometer scale dimensions[16−18] for applications at optical frequencies. The bowtie apertures have the similar inherent "high-efficiency radiation" and "superconfinement" properties as the bowtie antenna and, in addition, are capable of blocking the background light by taking advantage of an opaque metal screen. For the bowtie aperture at resonance, the field intensity enhancement at the bowtie apex can be 15 000 times that of illumination field,[14] which is comparable to the bowtie antenna.[18] However, the actual performances of bowtie apertures and bowtie antennas will depend on the materials, geometry, wavelength, and fabrication techniques. Like C- and H-shaped ridge apertures, the bowtie apertures have a much longer cutoff wavelength than regular apertures.[10] Visible or UV light with proper polarization can pass through the bowtie aperture without experiencing much intensity decay. The transmitted light is mainly confined within the nanoscale gap region offering optical resolution far beyond the diffraction limit. The sharp tips further enhance the local electric field via either lightening rod effect or resonant excitation of localized surface plasmon.[14]

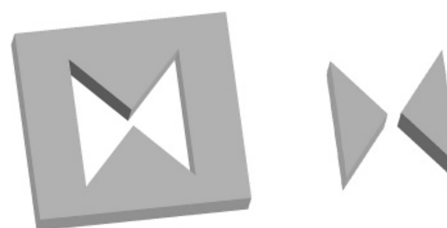

Figure 1. Schematics of bowtie aperture (left) and antenna (right). The gray areas represent metal film.

To our knowledge, experimental investigations of enhanced light transmission through bowtie aperture have not been reported in the literature. In this Letter, the advantages

* Corresponding author. E-mail: xxu@ecn.purdue.edu.

10.1021/nl052371p CCC: $33.50 © 2006 American Chemical Society
Published on Web 02/09/2006

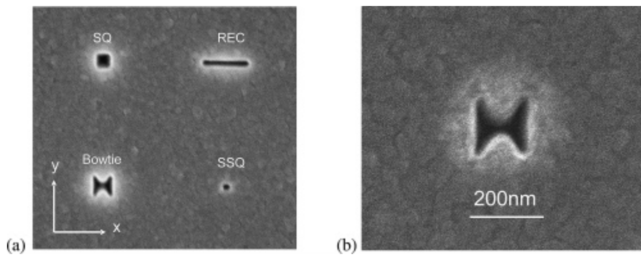

Figure 2. (a) SEM picture of the lithography mask pattern: Bowtie aperture with 135 nm × 155 nm outline size and 30 nm × 30 nm gap is fabricated on 150 nm thick aluminum film coated on a quartz substrate. Comparable apertures made in the array include a 100 nm × 100 nm square aperture (SQ) and 36 nm × 280 nm rectangular aperture (REC) of the same opening area and a 30 nm × 30 nm square aperture (SSQ) of the same gap size. (b) Zoom in SEM picture of the bowtie aperture.

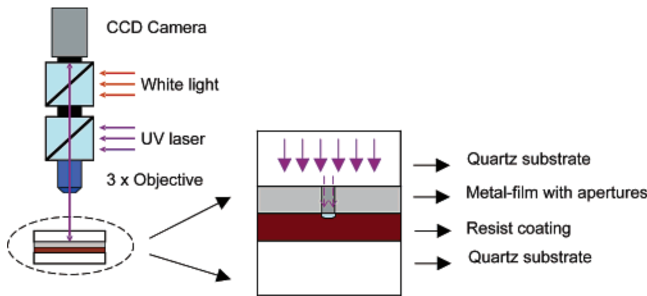

Figure 3. Schematic diagram of the experimental lithography setup.

of bowtie apertures for nanolithography are demonstrated by performing near-field photolithography experiments using a UV laser source. Sub-50-nm holes (about $\lambda/8$ of excitation wavelength) are produced in a positive photoresist-coated substrate by illuminating the mask containing the bowtie apertures. The lithography results clearly show that the bowtie aperture has much better performance than rectangular and square apertures in terms of high transmission and field localization.

The bowtie aperture is designed for high transmission and field localization at 355 nm laser wavelength using finite difference time domain (FDTD) calculations.[10,14] The gap between the tips should be as small as possible because it determines the size of the light spot.[13] It is also realized that a sharper tip provides better field enhancement.[13,14] Using the focused ion beam (FIB) milling technique, the smallest gap size and the radius of curvature that can be realized in this work are about 30 nm and 20 nm, respectively. Thin aluminum film is selected as the mask material because of its small skin depth (6.5 nm at 355 nm illumination) and high reflectivity (0.92 at normal incidence). The thickness of aluminum film was chosen to be 150 nm, sufficiently thick to block light through the film.

The lithography mask was fabricated on 12.7 mm × 12.7 mm × 5 mm (thick) optically flat (30 nm overall flatness) quartz wafers. A 150 nm aluminum thin film was deposited on the quartz substrate by electron-beam evaporation. The roughness of the aluminum film, measured using an atomic force microscope (AFM), was found to be less than 6 nm over a 5 μm × 5 μm area. The bowtie apertures and comparable regular apertures were then milled in the film (Figure 2a) by FIB nanopatterning (FEI Strata DB 235). The fabricated bowtie aperture has an outline dimension of 135 nm × 155 nm. The tapers at the apex form a full angle of about 80°, and the gap width of the aperture is around 30 nm. A comparable square aperture (SQ) (100 nm × 100 nm) and rectangular aperture (REC) (36 nm × 280 nm) with the same opening area as that of the bowtie aperture, and a small square aperture (SSQ) (30 nm × 30 nm) of the same size as the gap were made in an array pattern (Figure 2a) for the purpose of comparison.

Table 1. Lithography Results with Varying Exposure Times

	5 s exposure	2 s exposure	1.3 s exposure
bowtie (nm × nm)	150 × 180	70 × 80	40 × 50
SQ (nm × nm)	partially developed	not developed	not developed
SSQ (nm × nm)	not developed	not developed	not developed
REC (nm × nm)	250 × 400	220 × 280	220 × 220

Figure 3 shows the schematic diagram of the lithography setup, which is housed in a class-10 cleanroom rating glovebox to minimize contamination and to screen the environmental light from exposing the photoresist. A diode-pumped solid-state (DPSS) laser at 355 nm wavelength with linear polarization is used as the exposure source. With a 3 × UV objective, the laser beam is focused to a 110 μm spot over the mask. The polarization of the laser beam is directed across the gap of the bowtie aperture. The lithography experiments are performed by illuminating the bowtie apertures and comparable regular apertures shown in Figure 2 using the 110 μm diameter laser beam, i.e., under identical exposure conditions.

The positive photoresist (Shipley S1805) used in our experiments is measured to have a threshold exposure dose of about 7 mJ/cm^2 at $\lambda = 355$ nm using a lithography stepper and an aperture much larger than the wavelength. The regions exposed with a dose higher than that can be dissolved by rinsing in standard alkaline developer (Shipley M351) for 10 s, forming patterns in the photoresist. Because the incident laser intensity can be regarded as uniform over the small area of less than 1.5 μm × 1.5 μm over a 2 × 2 aperture array (shown in Figure 2), the shape, size, depth, and total volume of the holes in the photoresist essentially characterize the transmission properties of various nanoapertures in the mask.

The boundaries of the holes in photoresist formed by different apertures represent the regions where the dose equals the threshold exposure dose of the photoresist. Longer exposure time will result in larger and deeper holes in the photoresist, and thus it is important to precisely control the exposure dose in order to obtain nanoscale holes. (Note these are not through holes, but dimples.) The exposure time is controlled using an electric shutter with millisecond timing precision, while fixing the laser output power at a constant value. By variation of the exposure time between 1 and 5 s, small holes from tens of nanometer to hundreds of nanometer in size are produced in the photoresist by the bowtie aperture, the square aperture (SQ), and the rectangular aperture (REC). The smallest square (SSQ) aperture did not produce any holes

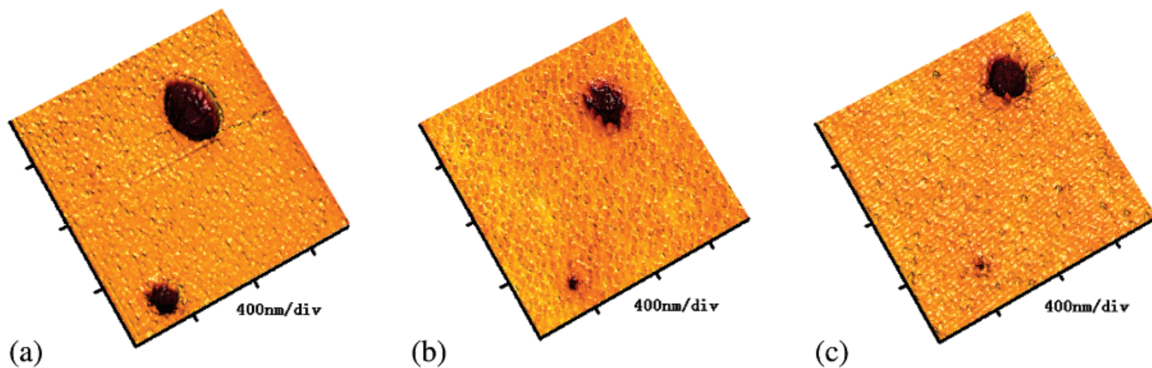

Figure 4. AFM pictures of lithography results corresponding to (a) 5 s exposure time, (b) 2 s exposure time, and (c) 1.3 s exposure time.

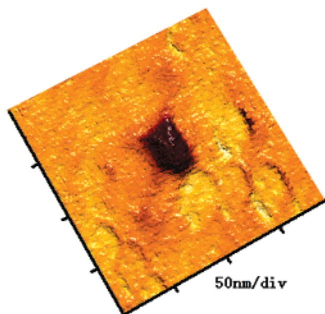

Figure 5. AFM image of 40 nm × 50 nm lithography hole produced by bowtie aperture at a 1.3 s exposure time.

on the photoresist. The lithography experimental results using 5, 2, and 1.3 s exposure time are summarized in Table 1.

With a 5-s exposure time, holes of sizes around 250 nm × 400 nm and 150 nm × 180 nm are formed by the rectangular aperture and the bowtie aperture, respectively. Figure 4a shows the corresponding atomic force microscopy (AFM) topography image of the holes in the photoresist produced by the aperture array on the mask as shown in Figure 2. Both the rectangular aperture and the bowtie aperture are overexposed because the lithography holes are larger than the outline dimensions of the mask apertures. Slight, irregular modification of the photoresist surface is barely observable at the position of the square aperture (SQ), and nothing is found at the position of the small square aperture (SSQ), indicating the transmitted peak intensity through these apertures was less than the threshold value. On the other hand, the propagation mode in the bowtie as well as in the rectangular aperture (note the width of the rectangle is larger than half of the wavelength) allows holes to be produced in the photoresist. Figure 4b shows the resist pattern at 2 s exposure. No surface modification is produced in the photoresist by the square apertures. The rectangular aperture (REC) produces a 220 nm × 280 nm hole. The size of the hole formed by the bowtie aperture is reduced to 70 nm × 80 nm. Figure 4c shows the patterns in the photoresist for an exposure time of 1.3 s. The hole formed by the bowtie aperture is further reduced to 40 nm × 50 nm in size, about $^1/_8$ of the excitation wavelength, and 16 nm in depth. An enlarged AFM image of the hole is shown in Figure 5. It is seen that the hole size is similar to the grain size of the thin aluminum film deposited on the quartz substrate. Further decreasing of the exposure time gave no results from the bowtie apertures.

To evaluate the consistency of the lithography results obtained by the bowtie aperture, a 2 × 2 bowtie aperture array as shown in Figure 6a is used. Experiments are repeated under the same exposure and developing conditions as described previously. An AFM image at 2 s exposure time is shown in Figure 6b. Four nano holes well below the diffraction limit are obtained. Their sizes are about 70 nm × 80 nm and have a size variation less than 10%. For 1.3 s exposure time, there is less consistency in the sizes of the holes obtained since for near threshold exposure, any variations in the exposure fluence, aperture size, etc., would cause a large change in the results.

FDTD calculations are carried out to further analyze the experimental data. Previous calculations have demonstrated enhanced optical transmission and nanoscale spatial resolution of C, H, and bowtie apertures.[9,10,14] In this calculation, a photoresist layer is added right below the metal film and a *y*-polarized, 355 nm wavelength light is used as the illumination source.

Figure 7 shows electrical field intensity distributions of the square, rectangular, and bowtie apertures in the *yz* plane across the center of the apertures. We see that an evanescent wave with an intensity decaying exponentially is found inside the square aperture. For the rectangular aperture, since its cutoff wavelength is longer than 355 nm, the propagation mode is seen in the aperture, therefore enabling higher intensity output. In addition, the transmitted field decays along the direction away from the two edges of the aperture, which is due to the scattering on the aperture edges. For the bowtie aperture, the transmitted light is concentrated in the gap region as seen in Figure 7c.

FDTD simulations, in conjunction with the experimental data, are used to find out the threshold dose needed for exposing the photoresist *through* the bowtie apertures, which are described as follows. The energy dose at the edge of the hole produced in the resist should represent the threshold value. To obtain the energy dose at the edge of the holes, FDTD calculations are conducted. The calculated intensity value (in W/cm^2) at the experimentally determined edge of the hole is multiplied by the experimental exposure time to obtain the exposure threshold dose (in J/cm^2). Applying a least-squares fitting procedure to the experimental data

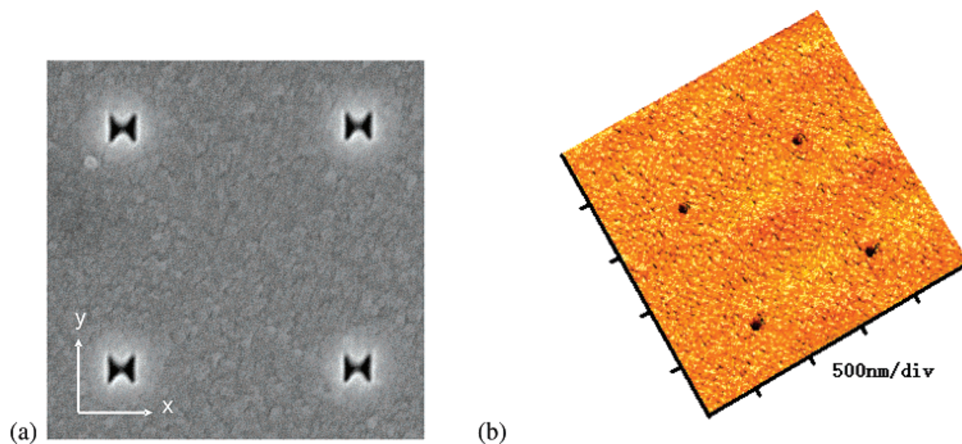

Figure 6. (a) SEM picture of 2 × 2 bowtie array on the mask. (b) AFM topography image of 2 × 2 bowtie array exposed for 2 s. Lithography holes are 70 nm × 80 nm with less than 10% variation in size.

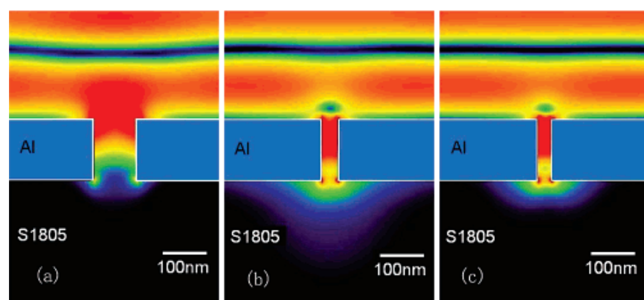

Figure 7. Electrical field intensity distribution of light propagating through (a) square, (b) rectangular, and (c) bowtie aperture in the cross section of the middle *yz* plane.

obtained for bowtie apertures at 5, 2, and 1.3 s of exposure times, we found a threshold dose of 18.2 mJ/cm^2, which is of the same order of the threshold value measured independently using a lithography stepper, 7 mJ/cm^2. This indicates that the bowtie apertures indeed provide a transmission efficiency of the order of 1. The difference could arise from a number of possibilities. First, the geometry of the bowtie used in the calculation may not be exactly the same as the actual bowtie used in experiments due to the uncertainty in measuring the size. Second, there might be a small separation between the bowtie and the photoresist caused by the roughness of the films (less than 6 nm), which is neglected in calculations. Third, the exposure used in nanolithography experiments is obtained under the near field condition when the field diverges quickly; whereas the threshold value obtained using a stepper is obtained using far field experiments.

In conclusion, nanolithography experiments have been performed to demonstrate the advantages of bowtie apertures over regular shape apertures in both transmission enhancement and nanoscale light concentration. Numerical simulations were used to explain experimental findings. Subdiffraction-limit lithography holes as small as 40 × 50 nm are obtained in the positive photoresist. This work shows that the bowtie apertures can be used as an alternative for nanolithography.

Acknowledgment. The financial support to this work by the Office of Naval Research and the National Science Foundation are acknowledged. Fabrications of aperture samples by FIB were carried out in the Center for Microanalysis of Materials, University of Illinois, which is partially supported by the U.S. Department of Energy.

References

(1) Aizenberg, J.; Rogers, J. A.; Paul, K. E.; Whitesides, G. M. *Appl. Phys. Lett.* **1997**, *71*, 3773−3775.
(2) Alkaisi, M. M.; Blaikie, R. J.; McNab, S. J.; Cheung, R.; Cumming, D. R. S. *Appl. Phys. Lett.* **1999**, *75*, 3560−3562.
(3) Chou, S. Y.; Krauss, P. R.; Renstrom, P. J. *Appl. Phys. Lett.* **1995**, *67*, 3114−3116.
(4) Davy, S.; Spajer, M. *Appl. Phys. Lett.* **1996**, *69*, 3306−3308.
(5) Srituravanich, W.; Fang, N.; Sun, C.; Luo, Q.; Zhang, X. *Nano Lett.* **2004**, *4*, 1085−1088.
(6) Luo, X. G.; Ishihara, T. *Appl. Phys. Lett.* **2004**, *84*, 4780−4782.
(7) Liu, Z.; Wei, Q.; Zhang, X. *Nano Lett.* **2005**, *5*, 957−961.
(8) Bethe, H. A. *Phys. Rev.* **1944,** *66*, 163−182.
(9) Shi, X.; Hesselink, L.; Thornton, R. L. *Opt. Lett.* **2003**, *28*, 1320−1322.
(10) Jin, E. X.; Xu, X. *Jpn. J. Appl. Phys.* **2004**, *43***,** 407−417.
(11) Chen, F.; Itagi, A.; Bain, J. A.; Stancil, D. D.; Schlesinger, T. E.; Stebounova, L.; Walker, G. C.; Akhremitchev, B. B. *Appl. Phys. Lett.* **2003**, *83***,** 3245−3247.
(12) Matteo, J. A.; Fromm, D. P.; Yuen, Y.; Schuck, P. J.; Moerner, W. E.; Hesselink, L. *Appl. Phys. Lett.* **2004**, *85***,** 648−650.
(13) Sendur, K.; Challener, W. *J. Microsc.* **2003**, *210*, 279−283.
(14) Jin, E. X.; Xu, X. *Appl. Phys. Lett.* **2005**, *86*, 111106.
(15) Grober, R. D.; Schoelkopf, R. J.; Prober, D. E. *Appl. Phys. Lett.* **1997**, *70*, 1354−1356.
(16) Farahani, J. N.; Pohl, D. W.; Eisler, H.-J.; Hecht, B. *Phys. Rev. Lett.* **2005**, *95*, 017402.
(17) Fromm, D. P.; Sundaramurthy, A.; Schuck, P. J.; Kino, G.; Moerner, W. E. *Nano Lett.* **2004**, *4*, 957−961.
(18) Schuck, P. J.; Fromm, D. P.; Sundaramurthy, A.; Kino, G. S.; Moerner, W. E. *Phys. Rev. Lett.* **2005**, *94*, 017402.

NL052371P